Journal of Power Sources 257 (2014) 380–387

Contents lists available at ScienceDirect

Journal of Power Sources

journal homepage: www.elsevier.com/locate/jpowsour

In situ atomic force microscopy nanoindentation of lithiated silicon nanopillars for lithium ion batteries

Quinn P. McAllister [a], Kenneth E. Strawhecker [a], Collin R. Becker [b,*], Cynthia A. Lundgren [b]

[a] *Weapons & Materials Research Directorate – Materials and Manufacturing Sciences Division, U.S. Army Research Laboratory, ATTN: RDRL-WMM-B, Aberdeen Proving Ground, MD 21005, USA*
[b] *Sensors and Electron Devices Directorate – Energy and Power Division, US Army Research Laboratory, ATTN: RDRL-SED-C, Adelphi, MD 20783, USA*

HIGHLIGHTS

- Nanoscale amorphous Si structures are fabricated with electron beam lithography.
- *In situ* mechanical measurements of a-Si are made during lithiation and delithiation.
- Mechanical properties of Si nanostructures are not recovered after 1 cycle.

GRAPHICAL ABSTRACT

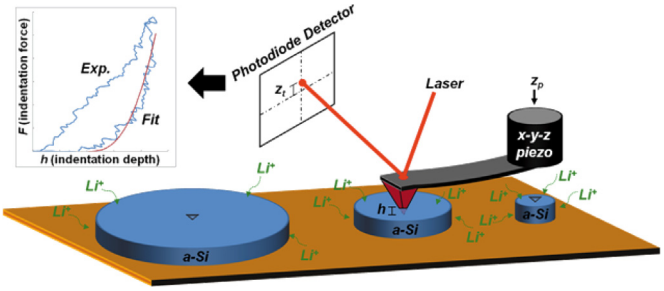

ARTICLE INFO

Article history:
Received 13 November 2013
Received in revised form
15 January 2014
Accepted 18 January 2014
Available online 28 January 2014

Keywords:
Lithium ion batteries
Silicon
Nanoindentation
Mechanical properties
AFM
Solid electrolyte interface

ABSTRACT

In this study, atomic force microscopy based nanoindentation techniques are used to measure the *in situ* mechanical properties of thin film, nanometer sized amorphous-silicon nanopillars (pillar diameters of 1000 nm, 500 nm, and 200 nm) at various stages of lithiation. The pillar indentation modulus and hardness are measured *ex situ* as-fabricated, *in situ* during lithiation at two different potentials (or stages of lithiation, 50 mV and 10 mV), and *in situ* after delithiation at 2 V. The measured modulus of the pristine amorphous silicon nanopillars was 74.7 ± 12.1 GPa. The hardness of the pristine pillars depended on depth and the contact conditions. In general, the mechanical properties of the nanopillars decreased with increased degrees of lithiation and only partially recovered upon delithiation. The inability of the silicon to recover the as fabricated mechanical properties indicates overall degradation of the pillar during only one lithiation–delithiation cycle, which could only be directly measured *in situ* using the employed atomic force microscopy based technique.

Published by Elsevier B.V.

1. Introduction

Silicon has the theoretical charge capacity (~4200 mAh g^{-1}) necessary to replace graphite (~372 mAh g^{-1}) as the state-of-the-art battery anode material [1–5]. However, the cyclability performance (i.e., capacity retention) of silicon anodes is limited by its massive volume expansion/contraction (up to ~300–400%) during lithiation-delithiation cycling that cracks the silicon-based anodes [2,3,5–7].

Historically, nanometer length scale silicon anodes have shown improved cyclability performance and resistance to failure versus larger anodes [2,3]. However, nanometer sized anodes can exhibit other structural changes during charge cycling, including wrinkling and porosity [8,9]. The authors previously observed that such microstructural changes cause mechanical degradation of

* Corresponding author. U.S. Army Research Laboratory, Electrochemistry Branch, 2800 Powder Mill Rd., Adelphi, MD 20783, USA.
E-mail address: collin.r.becker.civ@mail.mil (C.R. Becker).

0378-7753/$ – see front matter Published by Elsevier B.V.
http://dx.doi.org/10.1016/j.jpowsour.2014.01.077

nanometer scale pillars that were mechanically eroded by an AFM tip [10]. Prior studies on the correlation between *in situ* structural changes and anode performance have focused on morphological changes [8,9]. The mechanical properties of silicon anodes have primarily been studied *ex situ* while the *in situ* mechanical properties of nanometer sized silicon anodes have received limited attention [11–22]. The results of these studies were a large range of lithiated silicon moduli (the measured/predicted range was ~10–70 GPa with the majority in the 30–50 GPa range) [11–15,19–21], and may have missed nanoscale changes or gradients within a nanometer sized silicon anode (e.g., two phase lithiation). Atomic force microscopy (AFM) based indentation provides the necessary measurement length scale to interrogate nanometer sized anodes that the previously used techniques do not afford. The *in situ* mechanical properties of lithiated silicon anodes have not previously been studied using nanoindentation. Knowledge of the *in situ* mechanical properties of the silicon anodes is crucial to understanding the effect of cycling on the material performance.

In this study amorphous silicon (a-Si) thin film nanopillars were fabricated using electron beam lithography to have a height of 100 nm and diameters of 1000 nm, 500 nm, and 200 nm. *In situ* AFM-enabled indentation was used for the first time to measure the real-time properties of nanopillar anodes during the first charge–discharge cycle. A schematic of the experimental set-up is shown in Fig. 1. The AFM capability demonstrated and advancements made in this study motivate significant future research on the *in situ* properties of silicon and other advanced anode materials for future, high performance battery development.

Herein, the as-fabricated a-Si nanopillar mechanical properties were first measured *ex situ* prior to lithiation of the pillars to establish a baseline. These *ex situ* mechanical properties of pristine a-Si anodes deposited by electron beam evaporation are useful to both experimental and theoretical research that has previously provided a large range of measured values (i.e., ~45–141 GPa) [12,13,15–19,22]. To test the pillars *in situ* in the lithiated state, the sample was discharged to 50 mV and 10 mV potentials. Lithiated silicon may exhibit a phase transition below a 50 mV potential [2,6] and it was previously unknown if any dramatic mechanical property changes accompanied this transition. Therefore, further discharging of the sample to 10 mV gave a second degree of lithiation of the nanopillars. Lastly, the pillars were tested *in situ* in the delithiated state at a potential of 2 V. The indentations were made with an Agilent 5500 AFM equipped with a sapphire cantilever - diamond tipped probe (Micro Star Technologies) bent to three tip deflection voltages (z_t = 0.1 V, 0.3 V, and 0.5 V). As provided in the Experimental section, the tip deflection voltage (z_t) corresponds to a calibrated magnitude of applied force and indentation depth. Additional details on the sample preparation, indentation testing, and indentation analysis are also given in the Experimental section. The measured

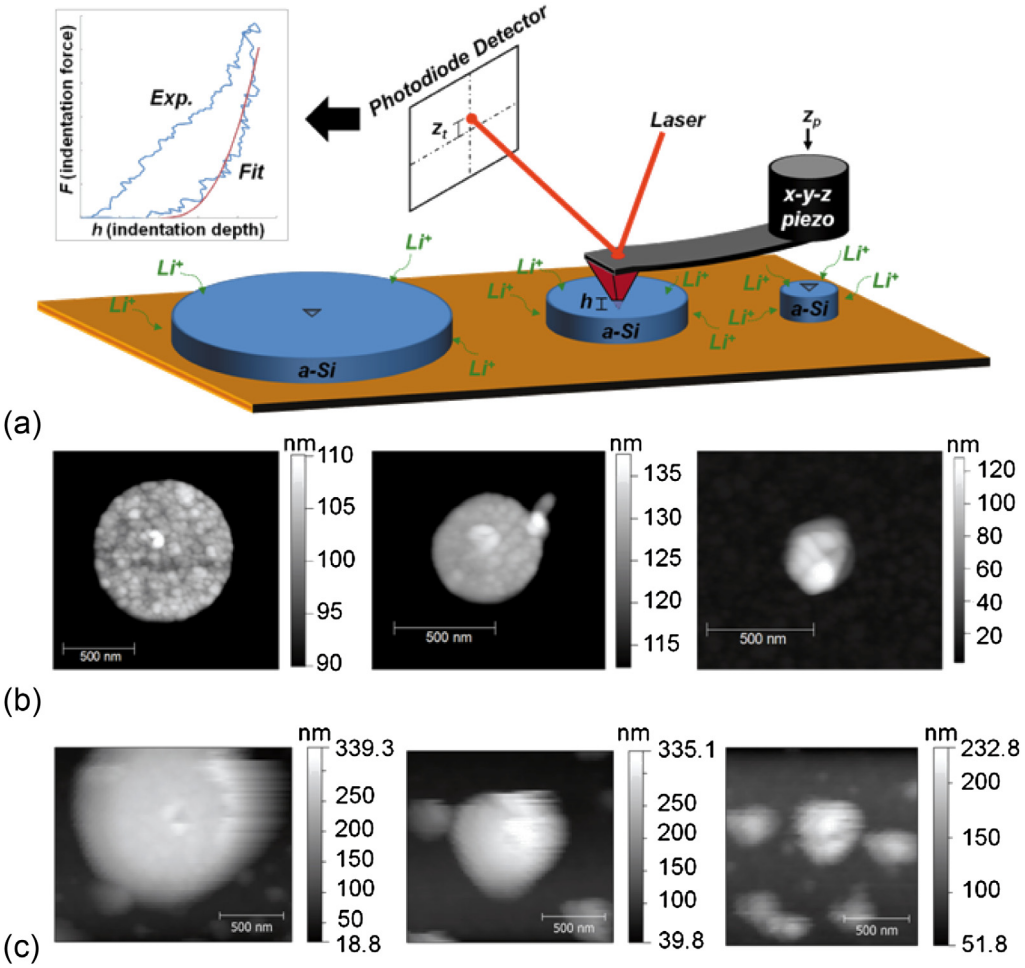

Fig. 1. a) A schematic of the experimental set-up for *in situ* AFM indentation of amorphous silicon (a-Si) nanopillar lithium ion battery anodes; b) Representative *ex situ* AFM indentations of (left to right) a 1000 nm (z_t = 0.3 V), 500 nm (z_t = 0.3 V), and 200 nm (z_t = 0.5 V) Si nanopillar; and c) Representative *in situ* AFM indentations of (left to right) a 1000 nm (z_t = 0.5 V), 500 nm (z_t = 0.3 V), and 200 nm (z_t = 0.5 V) nanopillar during the hold period at a 50 mV potential.

properties were then considered with respect to pillar diameter, degree of lithiation/delithiation, and depth to identify correlations between the first charge–discharge cycle, pillar size, and pillar degradation. The study herein clearly demonstrates the capability of AFM-enabled nanoindentation to measure the *in situ* mechanical properties of nanometer length scale battery anodes and specifically interrogated the mechanical property retention of a-Si nanopillars after the first charge–discharge cycle, providing invaluable insights for future LIB development.

2. Experimental

2.1. Materials and sample preparation

The a-Si nanopillars investigated in this study were fabricated on a substrate consisting of a 400 nm thick layer of nickel (Ni) on a (100) Si wafer. The Ni layer was electron beam evaporated onto the Si wafer using an Evatec BAK 641. After depositing the Ni, the substrate was patterned by electron beam lithography (Vistec EBPG5000 + ES) using a bi-layer poly(methyl methacrylate) (PMMA) photoresist. A 20 nm Ni adhesion layer followed by a 100 nm thick layer of a-Si were then deposited (also by electron beam evaporation) onto the patterned wafer, forming ~ 100 nm tall a-Si nanopillars. The pillars were spaced 2 μm apart center-to-center and had diameters of 1000 nm, 500 nm, and 200 nm. The *ex situ* indentation properties of the pristine, unlithiated nanopillars and the *in situ* properties of the lithiated/delithiated pillars were measured on separate samples (each consisting of 100 grids of 100×100 pillars). For the *in situ* measurements, the sample was enclosed in an electrochemical cell compatible with an Agilent 5500 AFM. The two electrode electrochemical cell consisted of the Si pillar sample as the working electrode and a lithium (Li) foil that served as both the counter and reference electrode (all voltages herein are in reference to the Li/Li^+ couple). The electrolyte employed in this study was a solution of 1 M lithium trifluoromethanesulfonate (chemical formula, CF_3SO_3Li, and trivial name, triflate) in propylene carbonate (PC). To limit exposure to moisture, the AFM was housed in a dry room with a dew point of less than −80 °C. The sample was first discharged at a rate of 1 mV s^{-1} from the open circuit voltage (~ 3.3 V; unlithiated) to 50 mV and held for approximately 1 h (1st lithiated state), at which point the morphological changes of the pillars had ceased. Subsequently, indentations were made on pillars of each diameter (see the following section for the indentation procedure). After completing the indentations (approximately 1 h), the sample was further discharged at 1 mV s^{-1} to 10 mV and held for approximately 1 h (2nd lithiated state). Following the hold, a different set of pillars was indented and the sample was charged back to 2 V (delithiated state). After a final c.a. 1 h hold, a final set of indentations was made on a third different set of pillars.

2.2. AFM Based nanoindentation of a-Si nanopillar anodes

The indentations were made with the Agilent 5500 AFM operated in "ramp" mode. The sapphire cantilever of the probe had a spring constant, k_c, of 604 N m^{-1}. The diamond indentation tip of the probe was a three-sided, irregular pyramid. The projected area of the tip (A_c) at a given contact depth (h_c) was calculated using the manufacturer provided geometric parameters and by estimating the three-sided pyramidal geometry as a simplified, equivalent rounded cone [21]. The relationship between A_c and h_c used in this study is given in Equation (1):

$$A_c = \begin{cases} \pi h_c(2r_{tip} - h_c) & h_c \le h^* \\ \pi \tan^2(\theta)(h_c + h_d)^2 & h_c \ge h^* \end{cases} \quad (1)$$

In Equation (1), r_{tip} is the radius of the rounded end of the cone (r_{tip} ~20 nm). The specified tip radius was "<20 nm." Therefore, the actual radius may be smaller than the 20 nm radius used herein and A_c may be slightly overestimated, leading to underestimation of the indentation properties. However, effective tip radius measurements made using a titanium roughness standard and NanoScope tip check software agreed with the manufacturer specifications – more details are provided in the Supplementary information); θ is the equivalent cone half-angle (θ ~29.75°); h_d is the distance between the apex of the rounded end of the cone and the apex of the same cone with an infinitely sharp tip (h_d ~ 20.3 nm); and h^* is the depth at which the probe transitions from the rounded spherical geometry to the conical geometry (h^* ~10.1 nm). Additional details about the rounded cone, or "spheroconical," probe area function and geometry are given elsewhere [23–25].

The indentations were made at a rate of 1 μm s^{-1} to three-different tip deflection voltages – 0.1 V, 0.3 V, and 0.5 V–by controlling the AFM piezo-scanner z-extension (z_p). There was no hold period between loading and unloading. The tip deflection voltage and z_p were converted to indentation force and indentation depth following established procedures [26]. The indentation force (F) and displacement (h) are given by Equations (2) and (3), respectively:

$$F = k_c z_t \quad (2)$$

$$h = z_p - z_t \quad (3)$$

In Equations (2) and (3), z_t is the tip deflection in nanometers (tip deflection is converted from voltage to nanometers through calibration [26]). To evaluate the indentation modulus (E_r) and indentation hardness (H), the measured indentation F–h curves were analyzed using the traditional Oliver–Pharr analysis [27] (i.e., the indentation unloading F–h curves were fit to a power law that was evaluated at h_{max} to calculate the elastic stiffness, S):

$$E_r = \frac{\pi^{1/2} S}{2\beta A_c^{1/2}} \quad (4)$$

$$H = \frac{F_{max}}{A_{c,max}} \quad (5)$$

In Equation (4), β is a constant that depends on probe geometry (e.g., $\beta = 1.034$ for a three-sided pyramidal Berkovich tip). E_r can be converted to sample modulus if the sample is isotropic with a known Poisson's ratio [27]. For the *ex situ* measurements, three indentations were made per pillar diameter and per tip deflection voltage. The novelty of this *in situ* measurement technique was limited by the number of indentations that could be conducted within the time at each lithiated state: ~1 h. Therefore, only one indentation per voltage and per pillar diameter was made at each *in situ* hold potential (i.e., 50 mV, 10 mV, and 2 V). In spite of this, the approach and results themselves are novel, shed light on previously unknown phenomena, and motivate significant future research. Every indentation was made on a separate pillar. The measured indentation properties were then analyzed with respect to the lithiated state and pillar diameter to elucidate key conclusions about the nanopillar lithiation and degradation processes.

3. Results and discussion

3.1. The ex situ properties of a-Si nanopillars

The indentations made on the 1000 nm and 500 nm pillars resulted in similar F–h curves, shown in Fig. 2, that were unaffected by any structural compliance effects (see Supplementary information). Therefore, the indentation hardnesses (H; Fig. 3b) and indentation moduli (E_r, Fig. 3a) measured for the 1000 nm and 500 nm pillars were representative of the pristine properties of the a-Si nanopillar anodes. It is important to note that the indentation properties of the 200 nm pillar could only be measured for the shallowest depths due to failure of the 200 nm pillars at greater depths. The observed failure of the 200 nm pillar highlights a key phenomenon of these pillars that is discussed further in the next section and the Supplementary information.

For both the 1000 nm and 500 nm pillars, the measured H increased with h (see Fig. 3b). The increase in H with h coincided with a decrease in the ratio of the final depth of indentation to the maximum depth of indentation, h_f/h_{max} (see Fig. 3c). The ratio h_f/h_{max} is a measure of the degree of plasticity of the indent. That is to say, the larger h_f/h_{max}, the more plastic the deformation during the indentation. Together, these trends of H and h_f/h_{max} with h suggest that the plastic stress distribution within the nanopillars was not in a fully developed state [21,28]. The measured H were therefore used for comparison to the *in situ* measurements but are limited in their accuracy of the absolute magnitude of the indentation hardness.

The indentation H measurements were sensitive to the plastic deformation that developed at the surface and directly around the indented region of the pillars [21,29,30]. The indentation E_r was more sensitive to the elastic response of the stresses/strains that developed deeper within the sample bulk [21,29,30]. E_r of the a-Si nanopillars was ~74.7 ± 12.1 GPa, which was measured independent of initial contact conditions (discussed in the Supplementary information) and pillar diameter using the two deeper sets of indentations made on the 1000 nm and 500 nm pillars. The measured E_r of the pristine a-Si pillars were within the range of prior measurements of a-Si (i.e., ~45–141 GPa) [12,13,15–19,22]. Combined with the analysis of E_r and H of the lithiated pillars in the next section, these results provide valuable insights on the evolution of the nanopillar surface and bulk properties in the lithiated and delithiated states.

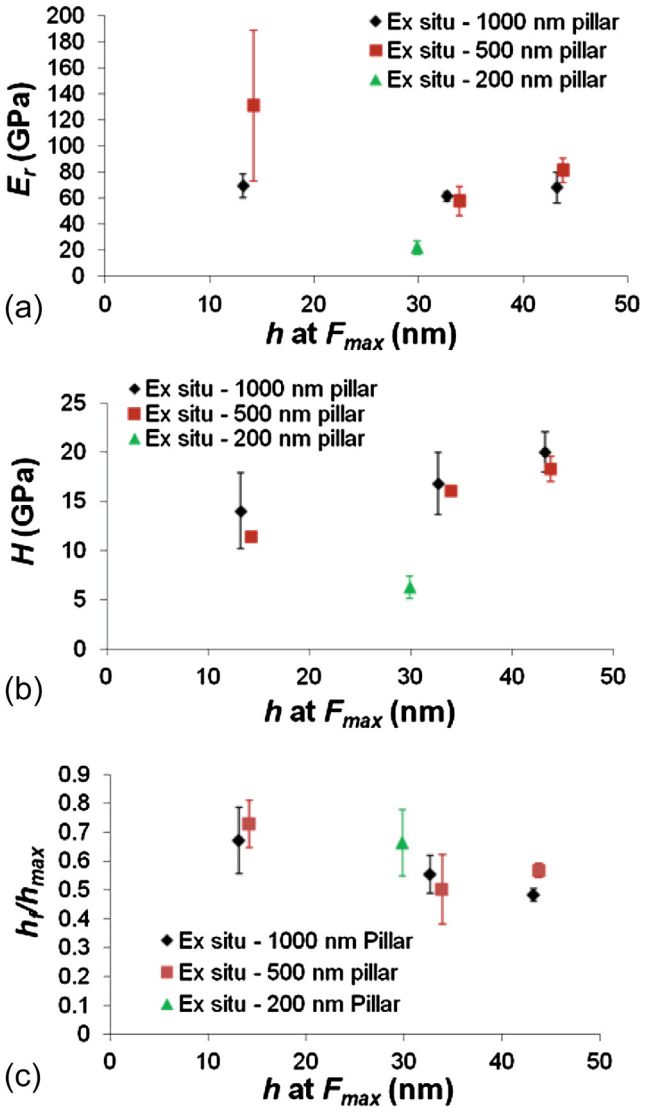

Fig. 3. Plots of (a) E_r, (b) H, and (c) h_f/h_{max} (h_{max} is h at F_{max}) versus h at F_{max} for indentations made *ex situ* on the 1000 nm, 500 nm, and 200 nm pillars.

3.2. Evolution of nanopillar indentation properties during lithiation–delithiation

To measure the mechanical properties of the lithiated pillars *in situ*, the sample was discharged from open circuit potential (OCP) to 50 mV in step "1" (first degree of lithiation); 50 mV–10 mV in step "2" (second degree of lithiation); and then charged (delithiated) from 10 mV to 2 V in step "3". During the first lithiation step to 50 mV (see "1" in Fig. 4), E_r and H of the 1000 nm pillar both decreased significantly – i.e., ~40–85% and ~60–70%, respectively. In fact, the 1000 nm pillar exhibited the lowest E_r for the shallowest indentation depth on each of the pillars at the 50 mV state (the open diamond symbol at an indentation depth of

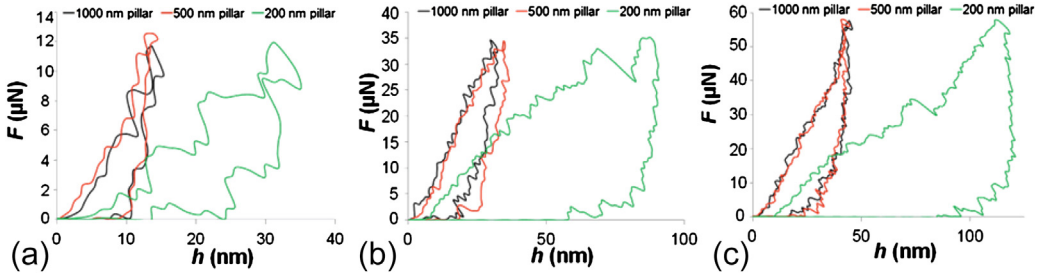

Fig. 2. Representative *ex situ* indentation force-displacement (F-h) curves of the 1000 nm pillars (black), 500 nm pillars (red), and 200 nm pillars (green) to three different tip deflection voltages (i.e., indentation forces): (a) 0.1 V, (b) 0.3 V, and (c) 0.5 V. (For interpretation of the references to colour in this figure legend, the reader is referred to the web version of this article.)

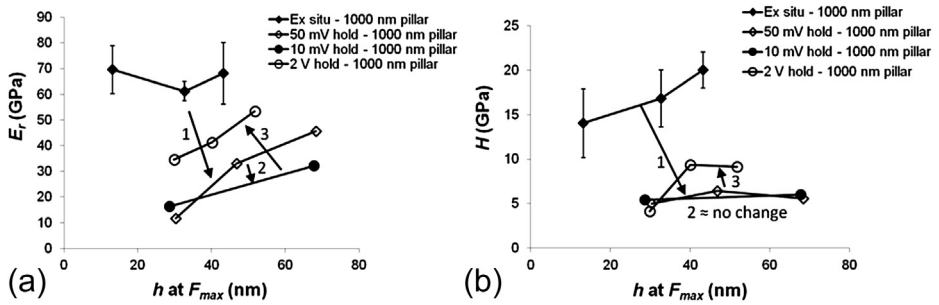

Fig. 4. The measured (a) E_r and (b) H as a function of h of the 1000 nm pillars for the *ex situ* and *in situ* states. The superimposed numbers – 1, 2, 3 – correspond to the arrows indicating the three steps in the discharge–charge cycle. The lines in the figures are not fitted curves and are intended only to guide the eye.

approximately 30 nm). E_r then increased with indentation depth while H (which is more sensitive to the plastic deformation that occurs closer to the surface [21,29,30]) remained low at all depths. Therefore, the observed trends of E_r and H with h for the 1000 nm pillar at the 50 mV lithiated state suggest that the properties were significantly decreased at the surface and less affected deeper into the pillar where the a-Si was less lithiated.

The measured decrease in the properties at the surface of the pillars could be due to a greater degree of lithiation of the pillar surface relative to the pillar bulk or the formation of a softer solid electrolyte interphase (SEI) layer [10,31–34]. Typically, the SEI exhibits a soft, fluffy region (primary SEI) that can be removed during AFM imaging, as is demonstrated on the nickel substrate in the Supplementary information [3,10,31,32,34]. In regards to the silicon nanopillars, an SEI layer was not readily apparent in a prior investigation [10] and AFM scans were conducted just prior to running the indentions that likely removed any unobserved primary SEI. A secondary SEI layer may also exist [34]. The properties/integrity of this second layer are not well understood; however, it is apparently very thin when using this particular 1 M triflate PC electrolyte [10]. Therefore, the measurements made to the shallowest depths may be affected by the secondary SEI layer (if it exists) and/or the lithium insertion into the surface. The apparently thin secondary SEI layer is not expected to influence measurements made deeper in the pillar bulk. Therefore, the measurements that were more dependent on the bulk response of the pillars, i.e., E_r measurements made at greater indentation depths, were primarily affected by the lithium insertion/extraction into/from the a-Si nanopillar anodes. The E_r of the lithiated/delithiated nanopillars measured in this study were consistent with the range of moduli previously predicted or measured for a variety of Li–Si alloys (the previously measured/predicted range is ~ 10–70 GPa with the majority in the 30–50 GPa range) [11–15,19–21].

Discharging the 1000 nm pillars to 10 mV (step "2" in Fig. 4; increasing the degree of lithiation) resulted in a further decrease of E_r (except for at the immediate surface, which may be an artifact of experimental variation or a result of unique surface effects). The H did not change outside of experimental variation relative to the 50 mV state, suggesting that the first lithiation step (50 mV) caused the maximum softening of the pillar surface and the second lithiation step (to 10 mV) primarily affected the pillar properties deeper into the pillar bulk (i.e., E_r). Such a property evolution may be overlooked by other characterization techniques with lower or no depth resolution. The increase of E_r with greater indentation depths suggests that an unaffected, or at least less affected, region within the pillar core still exists and the 1000 nm pillar was not completely lithiated. This result is consistent with prior observations, in which the pillars avoided fracture after one cycle and recovered a morphology very similar to their initial shape, as observed by *ex situ* SEM [10]. The total mass of Si pillars examined here is too low to allow accurate electrochemical measurement of the extent of lithiation of the pillars; however, previous *in situ* AFM experiments of silicon pillar lithiation concluded that at the voltage ramp used here of 1 mV s^{-1}, the 1000 nm pillar expanded by 231–256% volume (at 0.25 mV s^{-1} the pillars reached ~300%) [10]. This is less than the expected value of 310% for full lithiation and corroborates that the pillar is likely not completely lithiated [7]. An *in situ* TEM study of nanoscale amorphous Si particles have also observed instances of less than 300% volume expansion [35].

Upon delithiation (step "3" in Fig. 4), both E_r (modulus) and H (hardness) generally recovered. E_r approached the *ex situ* values at greater h but H remained below the H measured *ex situ*. The mechanical properties of the 1000 nm pillars therefore exhibited some recovery upon delithiation but were degraded at the pillar surface by the lithiation–delithiation cycle. A complimentary morphology study using *in situ* AFM and *ex situ* SEM showed the pillars remained intact after delithiation but with degraded mechanical properties, potentially from a decrease in density or induced porosity from cycling. The results herein corroborate those findings, motiving significant future research on the correlation between *in situ* morphology, *in situ* mechanical properties, and battery performance.

Similar to the 1000 nm pillars, the 500 nm pillars exhibited overall decreases in E_r (see Fig. 5a) and H (see Fig. 5b) when lithiated at 50 mV. The measured hardness (H) of the 500 nm pillars was approximately constant with depth and consistent with the hardness measured on the 1000 nm pillars at the 50 mV potential. Therefore, the first lithiation step resulted in a similar surface effect of the 1000 nm and 500 nm pillars. In contrast to the 1000 nm pillars, the modulus (E_r) of the 500 nm pillars did not increase with greater indentation depths. Instead, E_r plateaued approximately 55–75% lower than the E_r measured *ex situ*, suggesting an overall softening (or full lithiation) of the 500 nm pillars at the depths studied. Additional lithiation during discharge to 10 mV resulted in further decreases in both E_r (~70–75% total decrease from the *ex situ* measurement) and H (~65–85% total decrease from the *ex situ* measurement). Again, the property drops are approximately constant with increased indentation depth (within experimental variation), suggesting a further, overall softening and complete lithiation of the 500 nm pillars at the depths studied. Volume changes measured in a previous study also indicate full lithiation of the 500 nm pillar when lithiated at 0.25 mV s^{-1}, but have not been measured at the 1 mV s^{-1} rate used in this study [10]. The indenting probe used here is capable of recording low resolution images of the pillars so that a map can be constructed to "drive" the probe to a pillar and indent it. However, it cannot produce a fine enough image to record precise volume changes. Future work should include monitoring mechanical property changes as a function of lithiation rate concurrently with using a sharper probe to measure volume change at the various lithiation rates. While the hardness of the

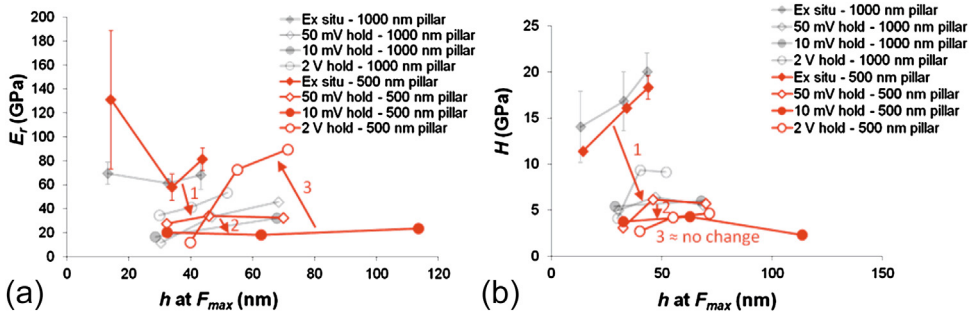

Fig. 5. The measured (a) E_r and (b) H as a function of h of the 500 nm pillars for the *ex situ* and *in situ* states. The superimposed numbers – 1, 2, 3 – correspond to the arrows indicating the three steps in the discharge–charge cycle. The results of the indentation measurements on the 1000 nm pillars, originally shown in Fig. 4, are faded in black for comparison.

500 nm pillars did generally decrease with the second lithiation step (in contrast to the 1000 nm pillar which remained approximately constant), the hardness at the shallowest depth may have increased from the 50 mV hold to the 10 mV hold.

Upon delithiation, the E_r and H at the surface of the 500 nm pillars decreased below the lithiated states, suggesting degradation of the mechanical properties of the 500 nm pillar surface due to the lithiation-delithiation cycle that was more significant than the degradation observed on the 1000 nm pillar. However, the E_r measured deeper in the 500 nm pillar recovered to the values measured *ex situ*. The recovery measured for the 500 nm pillars upon delithiation was the most significant of the three pillar diameters, which suggests an optimal pillar size exists for maximum battery life-cycle performance.

Similar to the *ex situ* measurements, the 200 nm pillars that were discharged to 50 mV and indented to 0.3 V and 0.5 V tip deflections (i.e., the two deeper indentations) cracked and failed. Therefore, only the E_r and H measured for the shallowest indentation depth ($z_t = 0.1$ V) are shown in Fig. 6. In spite of the growth of the pillar diameter during lithiation (see Supplementary information for additional explanation) [10], both E_r and H measured at the 50 mV hold decreased relative to the *ex situ* measurement. At the 10 mV state, the properties of the 200 nm pillars could be measured for the first two indentation depths because they did not cause catastrophic failure of the pillars. Discharging the 200 nm pillars to 10 mV resulted in a further decrease of E_r for a total decrease of ~ 90% of the *ex situ* measurement for indentations made to a tip deflection of 0.1 V. Similar to the 1000 nm and the 500 nm pillars, the hardness measured for the shallowest indentation on the 200 nm pillar increased from the 50 mV hold to the 10 mV hold then decreased with an increase in the indentation depth. The decreased indentation properties and the increased indentation depths of the lithiated 200 nm pillars suggest full lithiation of the 200 nm pillars at the depths studied. As with the 500 nm pillars, additional studies will be needed to record volume change of the pillars concurrently with the mechanical measurements to have a better gauge as to whether full lithiation is reached.

E_r of the 200 nm pillars in the delithiated state (open green circles in Fig. 6a) approached the *ex situ* measurements. However, when the indentation depth at F_{max} is considered, the 200 nm pillars showed minimal recovery upon delithiation. The indentation depths were around and often greater than the initial pillar height (~100 nm). The pillar height grew during lithiation, then recovered close to the initial pillar height after delithiation (within ~ 30% of the original pillar height). Therefore, from the results shown in Fig. 6 (open green circles), the conclusion can be made that the indentations easily penetrated through the pillar and were significantly influenced by the underlying, stiffer nickel substrate, resulting in the high measurements of E_r. The dramatic decrease in hardness of the 200 nm pillar in the delithiated state (see Fig. 6b) indicates that the density or internal structure of the 200 nm pillar has degraded severely and the insertion and removal of Li ions damages Si permanently. Therefore, capacity loss of Si may stem from Li that remains in the Si, induced porosity, cracking, and overall structural degradation. However, as other studies have explored, embedding Si particles in a conductive and mechanically supporting matrix or media could serve to alleviate effects of mechanical degradation of silicon during cycling [36–39]. Future *in situ* studies may investigate how Si particles change when surrounded by such media.

A non-intuitive size dependence of the mechanical property degradation of a-Si nanopillar anodes during the first lithiation-delithiation cycle was observed in this study. The smallest pillars studied herein, 200 nm diameter, withstood much less

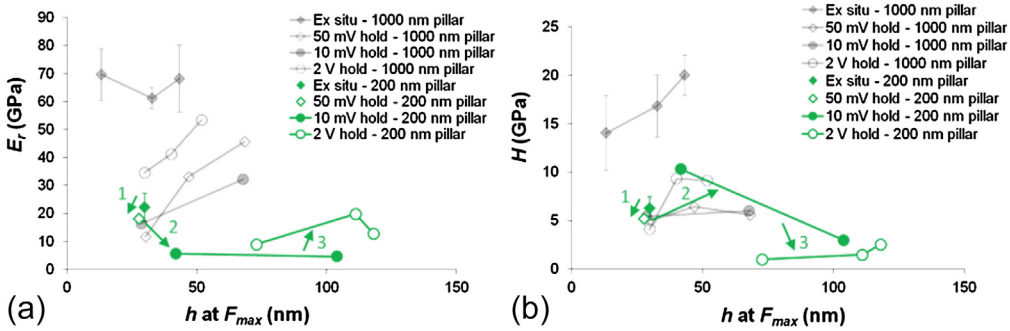

Fig. 6. The measured (a) E_r and (b) H as a function of h of the 200 nm pillars for the *ex situ* and *in situ* states. The superimposed numbers – 1, 2, 3 – correspond to the arrows indicating the three steps in the discharge–charge cycle. The results on the indentation measurements on the 1000 nm pillars, originally shown in Fig. 4, are faded for comparison.

indentation force during the first cycle relative to the pristine nanopillars, which was evident by the large indentation depth achieved by the indentations made in the lithiated and delithiated states. The dramatic decrease in load carrying capability is consistent with a significant decrease in the mechanical properties of the 200 nm nanopillars. The largest pillars studied herein, the 1000 nm pillars, exhibited a significant decrease in their indentation properties at the nanopillar surface (albeit not as significant as the 200 nm pillars). The indentation properties of the 1000 nm pillars increased with increasing depth and approached the *ex situ* measurements. The 500 nm diameter pillars, the intermediate diameter pillars studied herein, exhibited significant degradation at their surface (more significant than the 1000 nm pillars) but had the greatest measured recovery of the pillar bulk (i.e., the modulus measured for the deeper indentations). Therefore, an optimal pillar diameter might exist that limits the mechanical property degradation of a-Si nanopillar anodes during lithiation-delithiation cycling.

4. Conclusions

The performance of electronic systems for personal, commercial, or military use is often limited by the capacity and cyclability of the battery electrodes [1]. The high capacity of Si as an anode, if matched with high capacity cathodes, could revolutionize energy storage. However, silicon is pulverized and cracked during cycling, which causes capacity fade [2,3,5,7,11]. The propensity of silicon to crack during cycling depends on the *in situ* mechanical properties of silicon anodes [1]. In this study, the nanoscale *in situ* mechanical property retention of silicon nanopillar anodes during the first lithiation–delithiation cycle was studied for the first time using atomic force microscope-enabled nanoindentation. The indentation moduli, $E_{r,}$ and hardnesses, H, of three different pillar diameters – 1000 nm, 500 nm, and 200 nm – were measured *ex situ* on pristine amorphous silicon nanopillars and *in situ* at two different lithiated states and upon delithiation.

The results herein suggest that significant lithiation of larger nano- to micrometer sized Si pillar anodes occurs at the pillar surface, resulting in considerable degradation of the surface mechanical properties. The degradation at the surface of the largest pillar studied herein (1000 nm) extended into the pillar bulk, such that the as-fabricated, pristine pillar properties were not recovered for the indentation depths studied. Lithiation of smaller nanometer sized Si pillar anodes causes significant degradation of the Si–Si bonded structure and an overall decrease in their mechanical properties measured via indentation that were not previously observed using visually based experimental techniques. Finally, intermediate sized nanopillars exhibited significant surface degradation but maximum recovery of the bulk nanopillar properties, suggesting that an optimal pillar diameter exists for maximum retention of the mechanical properties of Si nanopillar battery electrodes. Identification of an optimal pillar diameter and pillar mechanical properties during multiple cycles are topics of ongoing and future research. The results of this investigation highlight the capability of AFM-enabled nanoindentation to overcome the challenges of *in situ* measurements and provide unparalleled, and previously unverified, insights into high performance, nanometer scale battery anodes.

Author contributions

The manuscript was written through contributions of all authors. All authors have given approval to the final version of the manuscript.

Funding sources

The authors are grateful to the Army Research Laboratory for financial support.

The research performed by QPM was supported in part by an appointment to the Postgraduate Research Participant Program at the U.S. Army Research Laboratory administered by the Oak Ridge Institute for Science and Education through an interagency agreement between the U.S. Department of Energy and USARL.

Acknowledgments

The authors gratefully acknowledge insightful discussion with Dr. J. Wolfenstine and Dr. J. Read. The authors would also like to acknowledge the financial support of the Army Research Laboratory. The research performed by QPM was supported in part by an appointment to the Postgraduate Research Participant Program at the U.S. Army Research Laboratory administered by the Oak Ridge Institute for Science and Education through an interagency agreement between the U.S. Department of Energy and USARL. The views and conclusions contained in this paper should not be interpreted as representing the official policies, either expressed or implied, of the Army Research Laboratory or the U.S. Government. The U.S. Government is authorized to reproduce and distribute reprints for Government purposes not withstanding any copyright notation herein.

Abbreviations

LIB	lithium ion battery
a-Si	amorphous silicon
AFM	atomic force microscope
Ni	nickel
Si	silicon
PMMA	poly(methyl methacrylate)
Li	lithium
PC	propylene carbonate

Appendix A. Supplementary data

Supplementary data related to this article can be found at http://dx.doi.org/10.1016/j.jpowsour.2014.01.077.

References

[1] J.M. Tarascon, M. Armand, Nature 414 (2001) 359.
[2] C.K. Chan, H. Peng, G. Liu, K. McIlwrath, X.F. Zhang, R.A. Huggins, Y. Cui, Nat. Nanotechnol. 3 (2008) 31.
[3] U. Kasavajjula, C. Wang, A.J. Appleby, J. Power Sources 163 (2007) 1003.
[4] P. Poizot, S. Laruelle, S. Grugeon, L. Dupont, J.M. Tarascon, J. Power Sources 97 (2001) 235.
[5] B. Philippe, R. Dedryvère, J. Allouche, F. Lindgren, M. Gorgoi, H. Rensmo, D. Gonbeau, K. Edström, Chem. Mater. 24 (2012) 1107.
[6] M.N. Obrovac, L.J. Krause, J. Electrochem. Soc. 154 (2007) A103.
[7] L.Y. Beaulieu, K.W. Eberman, R.L. Turner, L.J. Krause, J.R. Dahn, Electrochem. Solid State Lett. 4 (2001) A137.
[8] S. Iwamura, H. Nishihara, T. Kyotani, J. Power Sources 222 (2013) 400.
[9] X.H. Liu, S. Huang, S.T. Picraux, J. Li, T. Zhu, J.Y. Huang, Nano Lett. 11 (2011) 3991.
[10] C.R. Becker, K.E. Strawhecker, Q.P. McAllister, C.A. Lundgren, ACS Nano 7 (2013) 9173.
[11] A. Kushima, J.Y. Huang, J. Li, ACS Nano 6 (2012) 9425.
[12] V.A. Sethuraman, M.J. Chon, M. Shimshak, N. Van Winkle, P.R. Guduru, Electrochem. Commun. 12 (2010) 1614.
[13] S.T. Boles, A. Sedlmayr, O. Kraft, R. Mönig, Appl. Phys. Lett. 100 (2012) 243901.
[14] B. Hertzberg, J. Benson, G. Yushin, Electrochem. Commun. 13 (2011) 818.
[15] H. Kim, C.-Y. Chou, J.G. Ekerdt, G.S. Hwang, J. Phys. Chem. C. 115 (2011) 2514.
[16] R.J. Bondi, S. Lee, G.S. Hwang, Phys. Rev. B 81 (2010).
[17] D.-L. Liu, D.-X. Ye, F. Khan, F. Tang, B.-K. Lim, R.C. Picu, G.-C. Wang, T.-M. Lu, J. Nanosci. Nanotechnol. 3 (2003) 492.

[18] C. Gaire, D.-X. Ye, F. Tang, R.C. Picu, G.-C. Wang, T.-M. Lu, J. Nanosci. Nanotechnol. 5 (2005) 1893.
[19] V.B. Shenoy, P. Johari, Y. Qi, J. Power Sources 195 (2010) 6825.
[20] B. Gao, S. Sinha, L. Fleming, O. Zhou, Adv. Mater. 13 (2001) 816.
[21] A.C. Fischer-Cripps, Nanoindentation, Springer Science and Business Media, New York, 2002.
[22] L.B. Freund, S. Suresh, Thin Film Materials: Stress, Defect Formation and Surface, Cambridge University Press, Cambridge, 2003.
[23] Q.P. McAllister, The Energy Dissipative Mechanisms of the Particle-fiber Interface in a Textile Composite, University of Delaware, 2013.
[24] Q.P. McAllister, J.W. Gillespie Jr., M.R. VanLandingham, J. Mater. Res. 27 (2012) 197.
[25] M.R. VanLandingham, T.F. Juliano, M.J. Hagon, Meas. Sci. Technol. 16 (2005) 2173.
[26] M.R. Vanlandingham, S.H. McKnight, G.R. Palmese, R.F. Eduljee, J.W. Gillespie, J.R. McCulough, J. Mater. Sci. Lett. 16 (1997) 117.
[27] W.C. Oliver, G.M. Pharr, J. Mater. Res. 7 (1992) 1564.
[28] J.S. Field, M.V. Swain, J. Mater. Res. 8 (1993) 297.
[29] K.L. Johnson, Contact Mechanics, Cambridge University Press, New York, 1995.
[30] G. Feng, S. Qu, Y. Huang, W.D. Nix, Acta Mater. 55 (2007) 2929.
[31] M. Inaba, H. Tomiyasu, A. Tasaka, S.-K. Jeong, Z. Ogumi, Langmuir 20 (2004) 1348.
[32] D. Alliata, R. Kötz, P. Novák, H. Siegenthaler, Electrochem. Commun. 2 (2000) 436.
[33] I.T. Lucas, E. Pollak, R. Kostecki, Electrochem. Commun. 11 (2009) 2157.
[34] J. Zhang, R. Wang, X. Yang, W. Lu, X. Wu, X. Wang, H. Li, L. Chen, Nano Lett. 12 (2012) 2153.
[35] M.T. McDowell, S.W. Lee, J.T. Harris, B.A. Korgel, C. Wang, W.D. Nix, Y. Cui, Nano Lett. 13 (2013) 758.
[36] X. Zhou, L.-J. Wan, Y.-G. Guo, Small 9 (2013) 2684.
[37] K. Fu, O. Yildiz, H. Bhanushali, Y. Wang, K. Stano, L. Xue, X. Zhang, P.D. Bradford, Adv. Mater. 25 (2013) 5109.
[38] C. Loka, H. Yu, K.-S. Lee, J. Cho, J. Power Sources 244 (2013) 259.
[39] H.T. Yu, C. Loka, K.-S. Lee, J.S. Cho, S.H. Lee, Mater. Sci. Eng. B 178 (2013) 1422.